Cosmological test of an extended quintessence model

Gong Cheng,[1,2] Fengquan Wu,[1] and Xuelei Chen[1,2,3,4]

[1]*National Astronomical Observatories, Chinese Academy of Sciences, 20A Datun Road, Beijing 100101, China*

[2]*School of Astronomy and Space Science, University of Chinese Academy of Sciences, Beijing 100049, China*

[3]*Department of Physics, College of Sciences, Northeastern University, Shenyang 110819, China*

[4]*Center for High Energy Physics, Peking University, Beijing 100871, China*

(Received 29 January 2021; accepted 22 April 2021; published 19 May 2021)

We investigate the cosmological observational test of the extended quintessence model, i.e., a scalar-tensor gravity model with a scalar field potential serving as dark energy, by using the Planck 2018 cosmic microwave background (CMB) data, together with the baryon acoustic oscillations (BAO) and redshift-space distortion (RSD) data. As an example, we consider the model with a Brans-Dicke kinetic term $\frac{\omega(\phi)}{\phi}\phi_{;\mu}\phi^{;\mu}$ and a quadratic scalar potential $V(\phi) = A + B(\phi-\phi_0) + \frac{C}{2}(\phi-\phi_0)^2$, which reduces to general relativity (GR) in the limit $\omega(\phi) \to \infty$, and the cosmological constant in the limit $B = C = 0$. In such a model, the scalar field typically rolls down the potential and oscillates around the minimum of $V(\phi)$. We find that the model parameter estimate for the CMB + BAO + RSD data set is given by $\lg\alpha = -3.6^{+0.66}_{-0.54}(68\%)$ [α is defined in Eq. (3)], corresponding to $3.8\times10^5 < \omega_0 < 9.5\times10^7$ (68%) and $\lg C = 4.9 \pm 1.4$ (68%). However, the GR ΛCDM model can fit the data almost as good as this extended quintessence model and is favored by the Akaike information criterion. The variation of the gravitational constant since the epoch of Recombination is constrained to be $0.97 < G_{\rm rec}/G_0 < 1.03(1\sigma)$. In light of a recent report that the CMB data favor a closed universe, we consider the case with nonflat geometry in our fit and find that the mean value of Ω_k shifts a little bit from −0.049 to −0.036, and the parameters in our model are not degenerate with Ω_k.

DOI: 10.1103/PhysRevD.103.103527

I. INTRODUCTION

The scalar-tensor theories of gravity are extended relativistic theories of gravity. They can arise naturally as effective theories of the higher dimensional theories, for instance, the Kaluza-Klein theory, on four-dimensional spacetime [1]. They also provide a natural and simple framework to model the time variation of the gravitational constant via the dynamics of a scalar field [2]. In the scalar-tensor theory, the Ricci scalar couples to a scalar field. In its simplest version, the Brans-Dicke theory [3], a constant parameter ω is introduced. In the more general cases, ω can evolve with the Brans-Dicke field ϕ, and the potential of the Brans-Dicke field $V(\phi)$ should be considered. Such a scalar field may also be regarded as an extended quintessence model [4,5], i.e., a canonical scalar field which couples to gravity nonminimally, and can be used to explain the late-time cosmic acceleration [6].

The action of the extended quintessence model can be written as

$$S = \int \mathrm{d}^4x\sqrt{-g}\left[\frac{1}{2}F(Q)R - \frac{1}{2}Q^{;\mu}Q_{;\mu} - \tilde{V}(Q) + L_{\rm fluid}\right], \quad (1)$$

where $F(Q) = \frac{1}{8\pi G_0} + \xi(Q^2 - Q_0^2)$, and $Q_{;\mu}$ denotes covariant derivative of Q. Rewriting it in the Brans-Dicke form, $\phi \equiv 8\pi G_0 F(Q)$, and the transformed action is

$$S = \frac{1}{16\pi G_0}\int \mathrm{d}^4x\sqrt{-g}\left[\phi R - \frac{\omega(\phi)}{\phi}\phi_{;\mu}\phi^{;\mu} - V(\phi)\right] + S_{\rm m}(\Psi, g_{\mu\nu}), \quad (2)$$

where Ψ denotes the matter field. The dimensionless scalar field ϕ has a present day value ϕ_0, which is very close to 1, and its potential $V(\phi)$ is tightly constrained by observations. As $\omega(\phi) \to \infty$, the model reduces to general relativity (GR). As in the harmonic attractor model [2,7], we parametrize $\omega(\phi)$ as

$$2\omega(\phi) + 3 = \frac{1}{\alpha^2 - \beta\ln(\phi/\phi_0)}, \quad (3)$$

where α and β are model parameters. Note that at present day, $\phi \to \phi_0$, the model reduces to the GR case in the limits $\alpha \to 0$, $\beta \to 0$.

Here, we consider a model with an evolving scalar field potential $V(\phi)$, which is responsible for dark energy. We assume that the effective potential $V(\phi)$ can be expanded at the low orders as

$$V(\phi) = A + B(\phi - \phi_0) + \frac{C}{2}(\phi - \phi_0)^2. \tag{4}$$

In the limit $B \to 0$, $C \to 0$, the quintessence reduces to a cosmological constant with $A = \Lambda$.

The scalar tensor theory has been tested extensively with various astronomical observations. Solar system experiments have put strong constraints on Brans-Dicke theory up to $\omega > 40000$ at 2σ level [8]. Nonetheless, it is conceivable that gravity theory differs from GR in the early Universe, while it behaves like GR at present. It is therefore necessary to probe the behavior of gravity in different environments and scales, the cosmic evolution can provide a good laboratory to test gravity in the low density and low curvature regime, and the cosmic microwave background (CMB) data and large scale structure (LSS) data can be used to constrain such evolution [9,10]. While CMB provides the cleanest observational data, the geometrical redshift-distance relations measured by galaxy redshift surveys are useful for breaking the degeneracies in the CMB data. For the LSS, the simplest approach is to use the baryon acoustic oscillation (BAO) distance measurements, which we will use in the present paper, though there are also other approaches, for example, a measurement based on topology [11]. The redshift-distance relation as measured by standard candles such as the type Ia supernovae explosion is less reliable for this test, as the luminosity of the supernovae may depend on the gravitational constant, which varies in the scalar-tensor model, though such evolution has not been detected observationally [12]. In the present work, we will only use the distance measured with the CMB and LSS.

In addition, the growth of the structure is expected to be suppressed or enhanced in modified gravity compared to the standard GR model. So complementing distance measurements, the growth function is particularly sensitive to impose constraints on the modified gravity models [13].

The CMB data together with the LSS data had been used to constrain scalar-tensor models. In Ref. [14], the region of $-120.0 < \omega < 97.8$ was excluded at 2σ level by using WMAP 5 year data, other CMB experiments data and LSS data measured by the luminous red galaxy (LRG) survey of Sloan Digital Sky Survey (SDSS) data release 4. The constraint was improved to $\omega < -407.0$ or $\omega > 175.87$ by using *Planck* data [15]. Avilez and Skordis [16] reported $\omega > 1808$, by using *Planck* temperature and WMAP 9-year polarization data. Ooba *et al.* [2,7] obtained constraints on the harmonic attractor model, and some more recent constraints were given in [17–20]. In addition to the Brans-Dicke gravity, there have also been many investigations on more general classes of scalar-tensor models, such as the $f(R)$ gravity, early modified gravity [21,22], and the Horndeski gravity, which is the most general form with second-order field equations; see Refs. [23,24] for reviews. Note that these limits are dependent on the prior used, even for the same data, quite different limits can be derived with different priors.

The commencement of multimessenger astronomy with gravitational wave (GW) detection opens up a new window to test gravity theories. Based on the detections of GW signal produced by the binary neutron star merger (GW170817) [25] and its electromagnetic counterpart (gamma ray burst GRB170817A) [26,27], the speed of GW is constrained to be $c_{\rm T}^2 - 1 \lesssim 10^{-15}$. These measurements have several crucial implications for cosmological scalar-tensor theories [28–33]. As a result, the quartic and quintic Galileons are strongly excluded. The remaining viable models include simple Horndeski, e.g., Brans-Dicke and $f(R)$, and specific models beyond Horndeski theory, which is either conformally equivalent to theories with $c_{\rm T} = c$ or disformally fine-tuned.

Due to the vast number of gravity models in the market, it is important to test gravity in a model-independent way. In the past few years, several perturbation parametrizations are proposed and implemented in the Boltzmann solvers `CAMB` [34,35], such as `EFTCAMB` [36] and `MGCAMB` [37]. Although these formalisms cover a broad class of models, they have some limitations. There are a large number of free functions to be constrained, and simple parametrizations of these functions are unlikely to be successful, even missing the signature of modified gravity in the observations. Also, the connection between the formalism and physical models is not intuitive [38,39].

Most previous works on the scalar-tensor theory were performed for the cosmological model of flat geometry. Recently, it has been shown that the *Planck* CMB power spectra prefer a closed universe if the CMB lensing data are not used [40] for the models with gravity given by general relativity. The preference for the closed universe exists in both *Planck* 2015 and *Planck* 2018 data release and can not be removed by switching the likelihoods [41]. The positive curvature can explain the anomalous lensing amplitude $A_{\rm lens}$ but lead to the discordances for the local observations such as BAO. These discordances may originate from systematics or new physics. In Ref. [42], the constraint from Planck data and cosmic chronometers (CCs) gives $\Omega_k = -0.0054 \pm 0.0055$, without causing strong tension between Planck and CC data in the nonflat universe.

To constrain the model, we use the latest cosmological observations, including the CMB data together with BAO data and redshift-space distortion (RSD) data. We also investigate the curvature in this model to explore the possibility that the CMB temperature and polarization data might be compatible with the flat universe in the context of modified gravity, so that the discordances caused by the closed universe can be eliminated.

The rest of the paper is organized as follows: in Sec. II, we discuss the formalism of our computation, including background (II. A) and perturbation evolution (II. B), as well as numerical method (II. C). In Sec. III, we review the observational data used. We present our results in Sec. IV and conclude in Sev. V.

In this paper, we use natural units with $c = 1$. Following the convention of the CLASS code, all physical quantities are in unit of Mpc^n, so, for example, the units of $V(\phi)$, A, B, C, ρ, p are all Mpc^{-2}.

II. FORMALISM

The generalized Einstein equation and the equation of motion for the scalar field in this model are

$$\phi G_{\mu\nu} + \left[\Box\phi + \frac{1}{2}\frac{\omega(\phi)}{\phi}(\nabla\phi)^2 + \frac{1}{2}V(\phi)\right]g_{\mu\nu} - \nabla_\mu\nabla_\nu\phi - \frac{\omega(\phi)}{\phi}\nabla_\mu\phi\nabla_\nu\phi = 8\pi G_0 T_{\mu\nu}, \tag{5}$$

$$[2\omega(\phi)+3]\Box\phi + \frac{\mathrm{d}\omega(\phi)}{\mathrm{d}\phi}(\nabla\phi)^2 + 2V(\phi) - \phi\frac{\mathrm{d}V(\phi)}{\mathrm{d}\phi} = 8\pi G_0 T, \tag{6}$$

where T is the trace of the energy-momentum tensor. We use a perturbative approach to compute the observables in this model.

A. Background evolution

The equations governing the homogeneous background evolution of the Universe are

$$H = \frac{1}{a}\left[-\frac{\phi'}{2\phi} + \sqrt{\frac{a^2V}{6\phi} + \frac{a^2\rho}{\phi} + \frac{2\omega+3}{12}\left(\frac{\phi'}{\phi}\right)^2 - \kappa}\right], \tag{7}$$

$$H' = -\frac{3ap}{2\phi} - \frac{3}{2}\frac{a'^2}{a^3} - \frac{\kappa}{2a} - \frac{\phi''}{2a\phi} - \frac{a'}{a^2}\frac{\phi'}{\phi} - \frac{\omega\phi'^2}{4a\phi^2} + \frac{aV}{4\phi}, \tag{8}$$

$$\phi'' = -2\frac{a'}{a}\phi' + \frac{1}{2\omega+3}\times\left[3a^2(\rho-3p) + 2a^2V - a^2\phi\frac{\mathrm{d}V}{\mathrm{d}\phi} - \phi'^2\frac{\mathrm{d}\omega}{\mathrm{d}\phi}\right], \tag{9}$$

where the prime denotes the derivative with respect to the conformal time $\tau \equiv \int \mathrm{d}t/a(t)$, $H \equiv \frac{a'}{a^2}$ is the proper time Hubble rate, $\kappa = -\Omega_k H_0^2$ is a number characterizing the spacetime curvature in the cosmological model, and ρ and p are the rescaled total density and pressure of all matter components,

$$\rho = \frac{8\pi G_0}{3}\rho_{\mathrm{physical}}, \qquad p = \frac{8\pi G_0}{3}p_{\mathrm{physical}}.$$

The effective gravitational constant measured by Cavendish-type experiments is given by [3]

$$G(\phi) = \frac{G_0}{\phi}\frac{2\omega(\phi)+4}{2\omega(\phi)+3}, \tag{10}$$

so the value of ϕ at present day is set to be

$$\phi_0 = \frac{2\omega_0+4}{2\omega_0+3}. \tag{11}$$

Figure 1 shows the evolution of the scalar field ϕ for three models: the best-fit model obtained with the latest cosmological observations as detailed in the later sections, and the models with parameters $\lg C = 4.3$ and $\lg C = 4.7$. As we shall see later, all of these models are within the 1σ bound of $\lg C$.

The field ϕ began to increase after matter-radiation equality and converged to the present day ϕ_0. The corresponding evolutions of the generalized Brans-Dicke parameter $\omega(\phi)$ and the potential term $V(\phi)$ are plotted in the bottom panels of Fig. 1. Note that in all of these models the present day gravitation is indistinguishable from GR as $\omega(\phi)$ are high above the current solar system experimental limit. The scalar potential $V(\phi)$ decreases from a higher value to its present day value for the three example models shown in the figure. Its value at high redshift can be 1–3 orders of magnitude higher than the present day, so in these models, the dark energy can be important in the early evolution of the Universe.

In all the subplots of Fig. 1, the curves oscillated before converging to the present day value. It is easy to understand such oscillation behavior: the scalar field ϕ eventually settles down at the minimum of the potential, but near the bottom of the potential, it behaves like a damped oscillator. If we focus on the oscillatory terms containing ϕ'', ϕ', ϕ, and the dominant constant term, and neglect the other nonoscillatory terms of Eq. (9), the equation of motion reduces to a damped harmonic oscillator form,

$$\phi'' + 2Ha\phi' + k(\tau)(\phi - \phi_0) = 0, \tag{12}$$

where $k(\tau) = \frac{a^2}{2\omega+3}(C\phi_0 - B)$. If we take Ha, $k(\tau)$ as slowly varying, this can be solved analytically with the Wentzel-Kramers-Brillouin (WKB) approximation (see, e.g., [43]). To first order,

$$\phi(\tau) - \phi_0 = I_0 f(\tau)^{-\frac{1}{4}} e^{-\int Had\tau} \times \cos\left[\int_{\tau_2}^{\tau}\left(\sqrt{f(x)} - \frac{b(x)'}{4\sqrt{f(x)}}\right)dx\right], \tag{13}$$

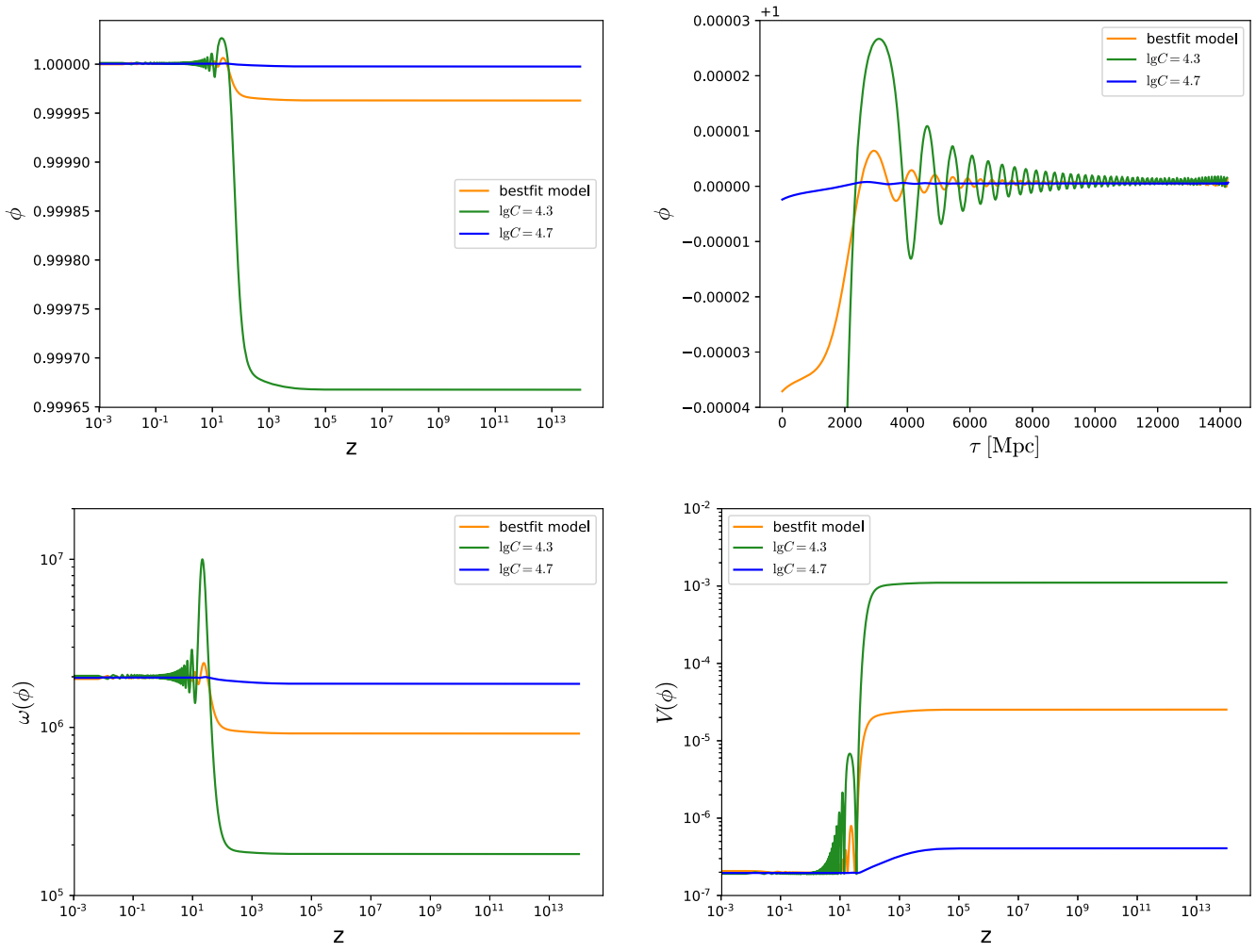

FIG. 1. Top left: The redshift evolution of the scalar field ϕ in a few of our extended quintessence models. The orange solid line represents the best-fit model with the CMB + BAO + RSD data set. The green and blue solid lines show models in which $\lg C$ is set to some selected values within the 1σ bound, while other parameters are set to the best-fit values. Top right: Evolution of ϕ with respect to the conformal time τ. Bottom left: Evolutions of the generalized Brans-Dicke parameter $\omega(\phi)$. Bottom right: Evolution of the scalar potential $V(\phi)$.

where I_0 is a constant, and

$$f(\tau) = \frac{a^2}{2\omega(\phi)+3}(C\phi_0 - B) - (aH)^2. \tag{14}$$

As $\phi_0 \approx 1$, $B \ll C$, and $(Ha)^2$ is also very small, these terms are negligible and

$$f(\tau) \approx \frac{a^2 C}{2\omega(\phi)+3}, \tag{15}$$

$$= a^2 C[\alpha^2 - \beta \ln(\phi/\phi_0)]. \tag{16}$$

where the last is obtained by substituting Eq. (3). Also,

$$e^{-\int Had\tau} = e^{-\int \frac{da}{a}} = a^{-1},$$

we then have approximately,

$$\phi(\tau) - \phi_0 \sim I_0 a^{-\frac{3}{2}}[C(\alpha^2 - \beta \ln(\phi/\phi_0))]^{-\frac{1}{4}} \times \cos\left[\sqrt{a^2 C(\alpha^2 - \beta \ln(\phi/\phi_0))}\tau + \psi\right]. \tag{17}$$

Compared with the oscillation term, the Hubble drag term is small, $H^2/\{C[\alpha^2 - \beta \ln(\phi/\phi_0)]\} \sim 7 \times 10^{-4}$, so the oscillation is underdamped. To examine the accuracy of this solution, we compare the period and amplitude obtained from the above analytical solution and the numerical solution. We take the model $\lg C = 4.3$ (the green line in Fig. 1) as an example. The conformal period estimated from Eq. (17) at $z = 5$ ($c\tau = 6206$ Mpc) is $cT = 537.3$ Mpc, which agrees well with the 539.6 Mpc as measured from the numerical solution. The ratio of amplitude between first and second peak estimated from the above equation is

about 4.2, while the one obtained from numerical solution is 2.7.

These oscillations occur mostly at high redshifts, and the amplitude for the $\omega(\phi)$ and $V(\phi)$ dropped low at low redshift. Nevertheless, they may be observable in high redshift precision observations in the future.

B. Perturbation evolution

In perturbation theory, $g_{\mu\nu} = a^2(\gamma_{\mu\nu} + h_{\mu\nu})$, where $\gamma_{\mu\nu} = \mathrm{diag}(-1, 1, 1, 1)$ and $h_{\mu\nu}$ are, respectively, the unperturbed and perturbed part of the metric. We choose to work in the synchronous gauge, where $h_{00} = h_{0i} = 0$, and follow the formalisms developed in Refs. [44–47]. The perturbations could be decomposed into the eigentensors of the Laplacian $\nabla^2 Q^{(m)} = -k^2 Q^{(m)}$,

$$h_{ij} = \sum_m 2h_L Q^{(m)}\gamma_{ij} + 2h_T Q^{(m)}_{ij} \tag{18}$$

$$= \sum_m \frac{h}{3} Q^{(m)}\gamma_{ij} - (6\eta + h)Q^{(m)}_{ij}, \tag{19}$$

$$\delta\phi = \sum_m \chi^{(m)} Q^{(m)}. \tag{20}$$

The stress energy tensor can be expressed as $T_{\mu\nu} = \bar{T}_{\mu\nu} + \delta T_{\mu\nu}$, and the unperturbed components are $\bar{T}^0{}_0 = -\rho$, $\bar{T}^0{}_i = \bar{T}^i{}_0 = 0$, and $\bar{T}^i{}_j = p\delta^i{}_j$. The stress energy perturbations can likewise be decomposed as

$$\delta T^0{}_0 = -\sum_m \delta\rho^{(m)} Q^{(m)}, \tag{21}$$

$$\delta T^0{}_i = \sum_m \frac{(\rho + p)\theta^{(m)}}{k} Q^{(m)}_i, \tag{22}$$

$$\delta T^i{}_0 = -\sum_m \frac{(\rho + p)\theta^{(m)}}{k} Q^{(m)i}, \tag{23}$$

$$\delta T^i{}_j = \sum_m \delta p^{(m)}\delta^i{}_j Q^{(m)} + \frac{3}{2}(\rho + p)\sigma^{(m)} Q^{(m)i}{}_j. \tag{24}$$

If we only consider the scalar perturbations, the perturbed equations read

$$h' = \left[k^2 s^2\eta + \frac{3a^2}{2\phi}\delta\rho - \frac{w\phi'^2\chi}{2\phi^3} + \frac{1}{\phi^2}\left(-\frac{3}{2}a^2\rho\chi + \frac{\phi'^2 \mathrm{d}\omega}{4\mathrm{d}\phi}\chi + \frac{\omega\phi'\chi'}{2} + \frac{3a'}{2a}\phi'\chi - \frac{1}{4}a^2 V\chi\right) + \frac{1}{\phi}\left(-\frac{1}{2}k^2\chi - \frac{3a'}{2a}\chi' + \frac{a^2 \mathrm{d}V}{4\mathrm{d}\phi}\chi\right)\right]\left(\frac{a'}{2a} + \frac{\phi'}{4\phi}\right)^{-1}, \tag{25}$$

$$\eta' = \left\{\frac{3a^2}{2\phi}(\rho + p)\theta + \frac{1}{2}\kappa h' + k^2\left[\frac{\omega\phi'\chi}{2\phi^2} + \frac{1}{2\phi}\left(\chi' - \frac{a'\chi}{a}\right)\right]\right\}\frac{1}{k^2 s^2}, \tag{26}$$

$$h'' = -\left(2\frac{a'}{a} + \frac{\phi'}{\phi}\right)h' + 2k^2 s^2\eta - \frac{9a^2}{\phi}\delta p + \frac{9a^2\chi}{\phi^2}p + \frac{3\phi'^2\omega\chi}{\phi^3} + \frac{1}{\phi^2}\left(-\frac{3\mathrm{d}\omega}{2\mathrm{d}\phi}\phi'^2\chi - 3\omega\phi'\chi' + 3\phi''\chi - \frac{3}{2}a^2 V\chi + 3\frac{a'}{a}\phi'\chi\right) + \frac{1}{\phi}\left(-3\chi'' - 3\frac{a'}{a}\chi' + \frac{3a^2 \mathrm{d}V}{2\mathrm{d}\phi}\chi - 2k^2\chi\right), \tag{27}$$

$$\alpha' = -\left(2\frac{a'}{a} + \frac{\phi'}{\phi}\right)\alpha + \eta - \frac{9a^2}{2k^2\phi}(\rho + p)\sigma - \frac{\chi}{\phi}, \tag{28}$$

$$\chi'' = -2\frac{a'}{a}\chi' - k^2\chi - \frac{1}{2}\phi' h' + \frac{1}{2\omega + 3}\left[-2\frac{\mathrm{d}\omega}{\mathrm{d}\phi}\chi\left(\phi'' + 2\frac{a'}{a}\phi'\right) - \frac{\mathrm{d}^2\omega}{\mathrm{d}\phi^2}\phi'^2\chi - 2\frac{\mathrm{d}\omega}{\mathrm{d}\phi}\chi'\phi' + a^2\frac{\mathrm{d}V}{\mathrm{d}\phi}\chi - a^2\frac{\mathrm{d}^2 V}{\mathrm{d}\phi^2}\phi\chi + 3a^2(\delta\rho - 3\delta p)\right], \tag{29}$$

where $s^2 = 1 - \frac{3\kappa}{k^2}$ and $\alpha = (h' + 6\eta')/2k^2$.

C. Numerical methods

We modify the publicly available Boltzmann code CLASS to numerically solve the equations above and compute CMB temperature and polarization anisotropy.

To recover the present day value of the effective gravitational constant given by Eq. (11), we use a "shooting" algorithm [9]; i.e., we evolve the background evolution equation from a very early time with a set of given model parameters and initial value of the scalar field ϕ_i to the present day time, ϕ_i is adjusted gradually until the Eq. (11) is satisfied to the required precision. In each "shooting," the model parameters that affect the background dynamics must be specified; these include the spatial curvature Ω_k, the total nonrelativistic matter density Ω_m, the Hubble constant H_0, gravity parameters α, β, and the scalar parameters A, B, C, and the second order differential equation also requires the initial values of the field ϕ_i and ϕ'_i. However, as in many quintessence models, the ϕ' damps to a "terminal velocity" at a later time, so that within a plausible range ϕ'_i practically does not affect the result. Of course, when the deviation is too large, there would be no ϕ_i that could yield the desired solution, but the solution could be found if the deviation from GR is within a reasonable range. In the simplest Brans-Dicke

model, ϕ_0 increases monotonically with ϕ_i. However, in the present model, the evolution of ϕ is more complicated. As a result, in some parameter space, more than one ϕ_i can evolve to the same desired ϕ_0. For this case, we choose the one which is closest to ϕ_0.

Also, at $z = 0$, the left-hand side (lhs) of Eq. (7) reduces to H_0, and if we neglect the kinetic term (the first term) in the right-hand side (rhs) of Eq. (7), which is only of the order $\sim 10^{-6}$ of the second term, we see this determines the value of $V(\phi)$, which in turn determines almost completely the value of A, which must be numerically very close to the cosmological constant in the cold dark matter (ΛCDM) model. We update ϕ_0' and A by the iteration process in the "shooting" algorithm.

In order to constrain the parameters in the gravity model with observations, we use the publicly available code Monte PYTHON [48,49], which adopts the Markov chain Monte Carlo (MCMC) method to explore the parameter space and obtain a Bayesian estimate of the parameters. At each point in the parameter space, the form of the potential $V(\phi)$ must be specified for CLASS to make the background run.

The parameters that varied in the Markov chains are the dynamical parameters listed above (Ω_k, H_0, α, β, B, C, matter physical density $\omega_m = \Omega_m h^2$, where h is defined by $H_0 = 100\ h\,\mathrm{km\,s^{-1}\,Mpc^{-1}}$), and the baryon physical density $\omega_\mathrm{b} = \Omega_b h^2$, (the cold dark matter physical density is given by $\omega_\mathrm{cdm} = \Omega_\mathrm{cdm} h^2 = \omega_m - \omega_\mathrm{b}$), the amplitude of scalar perturbations $\ln 10^{10} A_s$, the spectral index for scalar perturbations n_s, and the reionization optical depth τ_reio. Following the *Planck* analysis, we assume two massless and one massive neutrinos with mass $m = 0.06$ eV in this paper. We have also checked that if assuming three massless neutrinos; the results only have minor changes.

To avoid deviating too much in parameter space that could derail the code running, we set the priors as

$$\begin{aligned} \lg\alpha &\in (-6, -1), \\ \beta &\in (0, 1), \\ B &\in (-0.1, 0.1), \\ \lg C &\in (-10, 20). \end{aligned}$$

Note that the limits derived with the Bayesian method is dependent on the priors. The limits derived for priors with the linear and logarithmic distribution can be different. Here we adopt the logarithmic prior for α, this allow us to measure its posterior distribution near $\alpha = 0$ in more detail. We note that the GR limit $\alpha = 0$ corresponds to $\lg\alpha = -\infty$, which can not be attained in the current range of parameter, and if the peak of distribution is close to the lower limit of $\lg\alpha$, it could be the GR limit is favored. We shall see later that fitting the observation data constrains these parameters to a range well within these bounds. In a trial run, we found that the data favor a positive C, which allow us to also take a logarithmic prior on C to explore a large range of its value.

TABLE I. Data points measured by BAO surveys used in this work.

Redshift	Measurement	Value	Surveys
0.106	$r_\mathrm{s}/D_\mathrm{V}$	0.327 ± 0.015	6dFGS
0.15	$D_\mathrm{V}/r_\mathrm{s}$	4.47 ± 0.16	SDSS DR7-MGS
0.35	$D_\mathrm{V}/r_\mathrm{s}$	9.11 ± 0.33	SDSS DR7-LRG
0.38	$D_\mathrm{M}(r_\mathrm{s,fid}/r_\mathrm{s})$	1518.4 ± 22.4	SDSS DR12-BOSS
0.38	$H(z)(r_\mathrm{s}/r_\mathrm{s,fid})$	81.51 ± 1.91	SDSS DR12-BOSS
0.51	$D_\mathrm{M}(r_\mathrm{s,fid}/r_\mathrm{s})$	1977.4 ± 26.5	SDSS DR12-BOSS
0.51	$H(z)(r_\mathrm{s}/r_\mathrm{s,fid})$	90.45 ± 1.94	SDSS DR12-BOSS
0.61	$D_\mathrm{M}(r_\mathrm{s,fid}/r_\mathrm{s})$	2283.2 ± 31.9	SDSS DR12-BOSS
0.61	$H(z)(r_\mathrm{s}/r_\mathrm{s,fid})$	97.26 ± 2.09	SDSS DR12-BOSS
1.52	$D_\mathrm{V}/r_\mathrm{s}$	26.005 ± 0.995	SDSS DR14

III. OBSERVATIONAL DATA

We use the primary CMB data from *Planck* 2018 [50,51], including the temperature spectrum (TT), polarization spectra (TE, EE), and lensing measurements.

We also use a compilation of BAO data and RSD data from galaxy redshift surveys. The BAO and RSD data adopted in this paper are identical with Ref. [52], including the measurements from the 6dF Galaxy Survey (6dFGS) [53,54], the Sloan Digital Sky Survey (SDSS) main galaxy sample (MGS) [55,56], the luminous red galaxy (LRG) [57,58], SDSS DR12-BOSS [59], SDSS DR14 [60,61], velocities from SNe [62], GAMA [63], WiggleZ [64], VIPERS [65], and FastSound [66].

Table I lists the BAO measurements used in this paper. D_V is a combination of the Hubble parameter $H(z)$ and the angular diameter distance $D_\mathrm{A}(z)$,

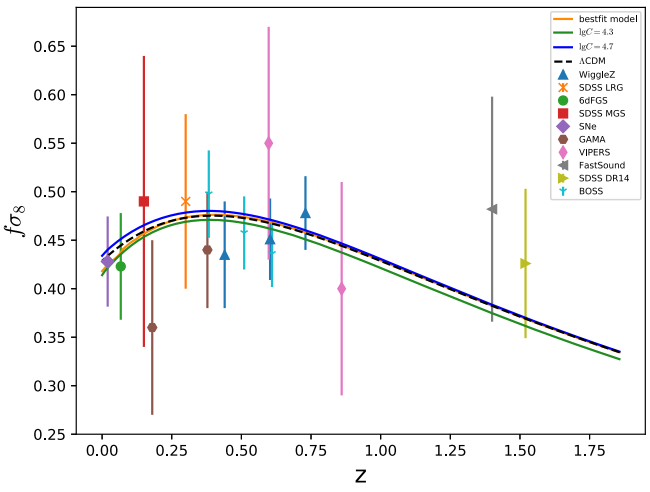

FIG. 2. The evolution of $f\sigma_8(z)$ with respect to the redshift z in the ΛCDM model (dashed black line) and the same scalar-tensor models as Fig. 1. The data points with error bars denote measurements from galaxy redshift surveys.

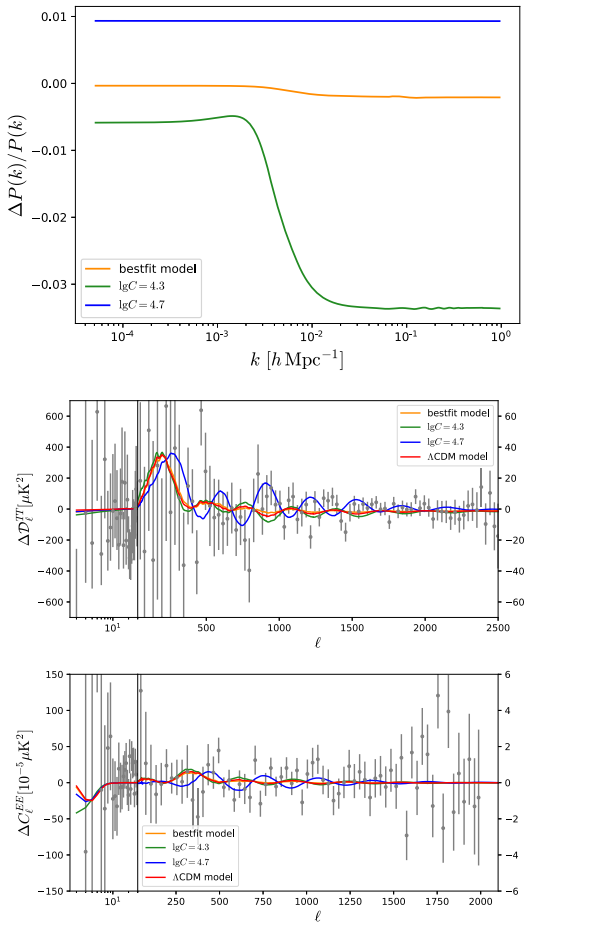

FIG. 3. The relative difference of the matter power spectrum (top panel), and the differences of the CMB temperature (middle panel) and EE polarization (bottom panel) angular power spectrum between the three scalar-tensor models and the ΛCDM model. For the CMB, we also plotted the Planck 2018 best fit model and the binned Planck measurements [69]. In order to present the result more clearly, the horizontal axis switches from log to linear at $\ell = 30$ as in Ref. [50], and we plot $\mathcal{D}_\ell = \frac{\ell(\ell+1)}{2\pi} C_\ell$ for TT spectrum and C_ℓ for EE spectrum.

$$D_{\rm V}(z) = \left[(1+z)^2 D_{\rm A}^2(z)\frac{cz}{H(z)}\right]^{1/3}, \tag{30}$$

while r_s is the comoving sound horizon at the end of the baryon drag epoch. Note that the fiducial value of r_s used by some observational groups is based on the analytical formula given by Eisenstein and Hu [67], and it is essential to replace it by the accurate value given by `CLASS`.

The RSD effect induced by the peculiar motion of galaxies can provide a powerful way to constrain the growth of structure. A large number of researches are conducted to measure the parameter combination $f(z)\sigma_8(z)$, in which the growth function is defined as

$$f(z) = \frac{{\rm d}\ln D}{{\rm d}\ln a}, \tag{31}$$

where $D(a) = \delta(a)/\delta(a_0)$ is the linear growth function. We plot the current RSD constraints on the growth function in Fig. 2. For the BOSS data, the measurements are $(1+z)D_{\rm A}(r_{\rm s,fid}/r_{\rm s})$, $H(z)(r_{\rm s}/r_{\rm s,fid})$, and $f\sigma_8$, and we use the full 9×9 covariance matrix to calculate the likelihood, so the correlation of $f\sigma_8$ among different redshift bins and the correlation between $F_{\rm AP}(z) = (1+z)D_{\rm A}H(z)/c$ and $f\sigma_8$ are taken into account. For the other RSD data, only the diagonal terms of the covariance matrix are used. For the WiggleZ data, as noted in Ref. [39], the points are conditionally plotted for the mean *Planck* cosmology according to the covariance matrix. In Ref. [68], the data points are rescaled by the ratios of $H(z)D_A(z)$ for the appropriate cosmology to take into account the Alcock-Paczynski (AP) effect. However, except for BOSS and WiggleZ, the measurements at low redshift are almost independent of cosmology models (e.g., 6dFGS and velocities from SNe), or the error bars are too large for this to matter. The AP effect correction $[\frac{H(z)D_{\rm A}(z)}{H(z)^{\rm fid}D_{\rm A}(z)^{\rm fid}} - 1]$ is about 0.8%, which is negligible compared with the RSD data error bar of 17%. We have checked and found that the total impact of AP effect and the nondiagonal terms of the covariance matrix on the

TABLE II. CMB constraints and CMB + BAO + RSD joint constraints on the parameters.

	CMB	CMB	CMB	CMB + BAO + RSD	CMB + BAO + RSD	CMB + BAO + RSD
Parameter	68% C.L.	95.4% C.L.	99.7% C.L.	68% C.L.	95.4% C.L.	99.7% C.L.
$\lg\alpha$	$-2.41^{+0.72}_{-0.65}$	$-2.4^{+1.4}_{-1.3}$	$-2.4^{+1.4}_{-2.2}$	$-3.59^{+0.66}_{-0.54}$	$-3.6^{+1.1}_{-1.2}$	$-3.6^{+1.7}_{-1.8}$
β	$0.253^{+0.13}_{-0.082}$	$0.25^{+0.17}_{-0.25}$	$0.25^{+0.29}_{-0.25}$	$0.16^{+0.044}_{-0.16}$	$0.16^{+0.29}_{-0.16}$	$0.16^{+0.46}_{-0.16}$
ω_0	$3.3\times10^4\,^{+6.3\times10^5}_{-3.2\times10^4}$	$3.3\times10^4\,^{+1.3\times10^7}_{-3.3\times10^4}$	$3.3\times10^4\,^{+8.3\times10^8}_{-3.3\times10^4}$	$7.6\times10^6\,^{+8.3\times10^7}_{-7.2\times10^6}$	$7.6\times10^6\,^{+1.9\times10^9}_{-7.5\times10^6}$	$7.6\times10^6\,^{+3.0\times10^{10}}_{-7.6\times10^6}$
10^7A	$1.11^{+0.62}_{-0.37}$	$1.11^{+0.92}_{-1.0}$	$1.1^{+1.2}_{-1.1}$	$1.993^{+0.21}_{-0.046}$	...	...
B	$0.0006^{+0.0045}_{-0.0034}$	$0.001^{+0.025}_{-0.024}$	$0.001^{+0.040}_{-0.034}$	$0.0011^{+0.0070}_{-0.0087}$	$0.001^{+0.025}_{-0.022}$	$0.001^{+0.050}_{-0.050}$
$\lg C$	$2.2^{+1.8}_{-1.7}$	$2.2^{+3.2}_{-3.3}$	$2.2^{+4.7}_{-3.8}$	$4.9^{+1.4}_{-1.4}$	$4.9^{+3.0}_{-2.8}$	$4.9^{+4.1}_{-4.8}$
$H_0[\mathrm{km\,s^{-1}\,Mpc^{-1}}]$	$56.9^{+3.0}_{-4.8}$	$56.9^{+8.7}_{-7.8}$	57^{+13}_{-10}	$67.5^{+1.2}_{-1.2}$	$67.5^{+2.5}_{-2.5}$	$67.5^{+4.1}_{-3.7}$
Ω_k	$-0.036^{+0.014}_{-0.015}$	$-0.036^{+0.031}_{-0.030}$	$-0.036^{+0.041}_{-0.043}$	$-0.0004^{+0.0031}_{-0.0029}$	$-0.0004^{+0.0060}_{-0.0063}$	$-0.0004^{+0.0090}_{-0.010}$

likelihood is about $\Delta \ln \mathcal{L} \sim 0.15$, so the correction due to AP effect is really small, and the overall effect to the final constraints is negligible. The best fit model preferred by CMB + BAO + RSD data set overlaps with the ΛCDM model at $z > 0.25$. As an example, we choose $\lg C = 4.3$, which is within the 1σ bounds. We find that it fits the RSD data points better than ΛCDM model, showing the ability of this model to provide a better fit to RSD data while being consistent with CMB + BAO data.

IV. RESULTS

In Fig. 3, we show the relative difference of matter power spectrum and the CMB temperature (TT) and polarization (EE) angular power spectrum between ΛCDM model and the three example models we use. The locations of the acoustic peaks shift to larger or smaller angular scales, depending on the parameters used. Note for these four models, the six cosmological parameters are set to be the same, so the ΛCDM model (red line) adopts

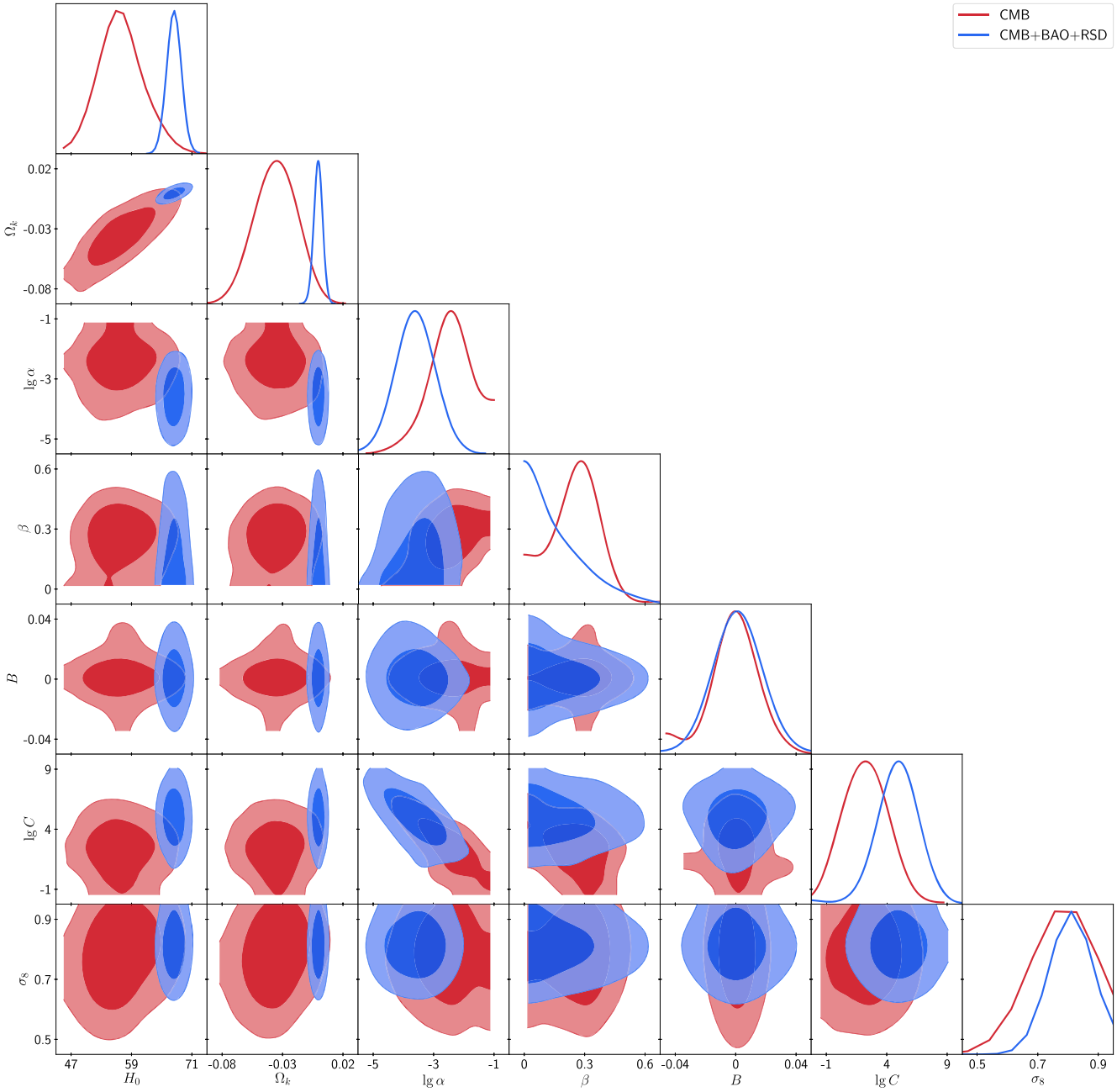

FIG. 4. The 68% and 95% confidence regions in the scalar-tensor model together with the 1D marginalized posterior distributions for the CMB and the CMB + BAO + RSD data sets.

different cosmological parameters from the Planck 2018 best fit model.

We can derive constraints on single parameters or joint constraints on two parameters after marginalizing over the other parameters. Table II lists the 1σ (68%), 2σ (95.4%), and 3σ (99.7%) credible intervals for the various parameters. Two cases are given: CMB only case, in which the *Planck* 2018 temperature and polarizations data are used in the fitting, and the CMB + BAO + RSD case, in which in addition to the CMB data, the *Planck* CMB lensing measurements and the BAO and RSD data set are also used. A is not very well constrained by the CMB + BAO + RSD data set, so only 1σ confidence region is given by MCMC.

To visualize the constraints from the observations, in Fig. 4, we also show the 68% and 95% credible level contours of each pair of parameters, and the 1D marginalized posterior distributions of each parameter. While the CMB data already constrained the parameters, the contours are tightened considerably with the additional BAO and RSD data, and the center of the contours are also shifted significantly. We found that although the best fit values of H_0 and σ_8 are nearly the same as the ΛCDM case, the corresponding errors are enhanced by a factor of 2–3, so in some sense, our model could potentially reduce the present tension in these parameters. Specifically, for our model, the constraint from CMB + BAO + RSD data set is $H_0 = 67.5 \pm 1.2\ \mathrm{km\,s^{-1}\,Mpc^{-1}}$, while for ΛCDM model, $H_0 = 67.50 \pm 0.59\ \mathrm{km\,s^{-1}\,Mpc^{-1}}$. And the constraint from SN Ia and geometric distances from Milky Way parallaxes and eclipsing binaries is $H_0 = 73.5 \pm 1.4\ \mathrm{km\,s^{-1}\,Mpc^{-1}}$ [70]. For the σ_8 tension, the constraint from CMB + BAO + RSD data set in our model is $S_8 \equiv \sigma_8(\Omega_m/0.3)^{0.5} = 0.822 \pm 0.036$ and $\Omega_m = 0.311 \pm 0.011$, while the ΛCDM model yields $S_8 = 0.827 \pm 0.011$, $\Omega_m = 0.3123 \pm 0.0068$, and DES-Y1 galaxy clustering, and the weak lensing data gives $S_8 = 0.773^{+0.026}_{-0.020}$ and $\Omega_m = 0.267^{+0.030}_{-0.017}$ [71].

Except for the parameter β, the 1D posterior distributions, we obtain all have narrow peaks well within the allowed range, so the result is not overtly dependent on the adopted prior. The β parameter distribution also has a peak, and for the CMB-only data, it is in the middle of the allowed range, but for the CMB + BAO + RSD data combination, the peak is near 0, which is the border of the prior.

We find good consistency with the ΛCDM model for the parameters β, A, and B. Interestingly, the fit gives a nonzero value for α, which deviates from the GR ΛCDM model limit ($\alpha = 0$) at the $>3\sigma$ level, but we should be very careful in interpreting this result. First, the corresponding ω value is quite large, so the deviation from the GR is in fact fairly small. Furthermore, if we inspect the value of the likelihood, the maximum logarithm likelihood values are −1391.87 and −1391.90 for our extended quintessence model and the GR ΛCDM model, respectively. This shows that the GR ΛCDM model can fit the data almost as good as our extended quintessence model. When only one parameter $\lg\alpha$ is singled out, it may appear that the best fit is several σ away from the GR limit (in our case, the minimum of $\lg\alpha$), but the Bayes estimator is obtained by integrating the posterior distribution over the parameter space, and this is not completely accurate for the GR ΛCDM model, which essentially has fewer parameters, i.e., lower dimensions. If we use the Akaike information criterion (AIC) to compare our model with the GR ΛCDM model [72,73],

$$\mathrm{AIC} = -2\ln\mathcal{L}_{\max} + 2k, \tag{32}$$

where k is the number of parameters, then the extended quintessence model is penalized for its additional four parameters, and the ΛCDM model would be the better model.

The data also favor a positive C, in which case the dark energy $V(\phi)$ is not constant but has an evolution. There is some degeneracy between the parameter C and α, as the $\alpha - C$ contour has a linear shape. This raises the possibility that the nonzero α best fit may be partially due to this degeneracy; i.e., the observation data favor a dark energy model, and due to the degeneracy, a nonzero α value is induced.

We can derive the variation of the gravitational constant G_{rec}/G_0 in this model, defined as the ratio of the gravitational constant during the recombination epoch and the present day. The 1σ bound from the CMB + BAO + RSD constraint is $0.97 < G_{\mathrm{rec}}/G_0 < 1.03$.

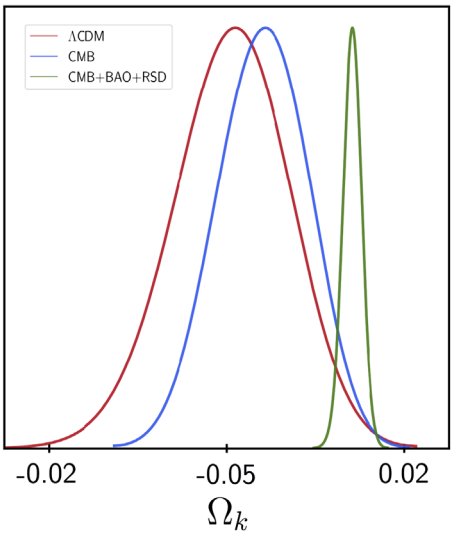

FIG. 5. The 1D marginalized posterior distributions of curvature. The red line represents the constraint from *Planck* 2018 temperature and polarization data for the nonflat ΛCDM model. The blue line shows the constraint from the same data but for our extended quintessence model. The green line shows the constraint on our model with the CMB + BAO + RSD data.

Finally, as we discussed earlier, in this work, we consider nonflat geometry for both the extended quintessence model and the GR ΛCDM model. Figure 5 shows the constraints on the curvature in our extended quintenssence model, compared with the ΛCDM model. As in ΛCDM model case, the closed model is also slightly favored by the *Planck* 2018 data in the scalar-tensor model. The flat universe case $\Omega_k = 0$ is still about 2σ from the best fit. The peak of the distribution shifts toward the flat limit a little bit, from -0.049 to -0.036. So in this extended quintessence model, the closed model is still a favored fit, only slightly closer to the flat case than the GR ΛCDM model.

V. SUMMARY

In this paper, we investigated a specific scalar-tensor theory, with a quadratic scalar potential, i.e., an extended quintessence model of dark energy. We parametrize the Brans-Dicke parameter in a form similar to the harmonic attractor model, then we follow the standard formalism to derive the background and perturbation equations. Constraints on the model parameters are derived by using a MCMC program, with the latest cosmological data, including the *Planck* 2018 CMB data, and the BAO and RSD data from various galaxy redshift surveys.

We found that in the quadratic potential extended quintessence model, the scalar field rolls down and oscillates around the minimum point of the potential $V(\phi)$. This behavior is typical, for the oscillation is underdamped. And its energy density can be several orders of magnitude higher than the present day value, so it may play a role even in the early Universe.

Our global fitting gives a statistically significant nonzero α and C values. This shows that at least the quadratic potential extended quintessence model considered here is allowed by current observations. However, we found that the maximum likelihood value is nearly the same for the GR ΛCDM model and our extended quintessence model. The nonzero value of α and C is partly because the GR ΛCDM model has fewer dimensions; hence, it is disadvantaged in the integration over parameter space. With less parameters, the GR ΛCDM model would be preferred with the Akaike information criterion. The best fit values of H_0 and σ_8 are similar to those obtained in the ΛCDM case; however, the errors are enhanced by a factor of 2–3. So in some sense, our model could partially alleviate the present tension in these parameters. The variation of the gravitational constant between the recombination epoch and the present day is constrained as $0.97 < G_{\rm rec}/G_0 < 1.03(1\sigma)$.

In addition, we have constrained the curvature Ω_k in this gravity model with only CMB data. Compared with ΛCDM model, the peak of the posterior distribution has a small shift from -0.049 to -0.036. This shows the possibility of alleviating the curvature problem raised recently in the context of modified gravity theories.

ACKNOWLEDGMENTS

We acknowledge the support of the Ministry of Science and Technology through Grant No. 2018YFE0120800, the National Natural Science Foundation of China through Grants No. 11633004, No. 11473044, No. 11773031, No. 11973047, and the Chinese Academy of Science Grants No. QYZDJ-SSW-SLH017, No. XDB 23040100, No. XDA15020200. The computation of this work has been carried out on TianHe-1(A) computer at the National Supercomputer Center in Tianjin, and the computers of the NAOC Astronomical Technology Center.

[1] T. Clifton, P. G. Ferreira, A. Padilla, and C. Skordis, Phys. Rep. **513**, 1 (2012).
[2] J. Ooba, K. Ichiki, T. Chiba, and N. Sugiyama, Phys. Rev. D **93**, 122002 (2016).
[3] C. Brans and R. H. Dicke, Phys. Rev. **124**, 925 (1961).
[4] F. Perrotta, C. Baccigalupi, and S. Matarrese, Phys. Rev. D **61**, 023507 (1999).
[5] X. Chen, R. J. Scherrer, and G. Steigman, Phys. Rev. D **63**, 123504 (2001).
[6] S. Tsujikawa, Classical Quantum Gravity **30**, 214003 (2013).
[7] J. Ooba, K. Ichiki, T. Chiba, and N. Sugiyama, Prog. Theor. Exp. Phys. **2017**, 043E03 (2017).
[8] B. Bertotti, L. Iess, and P. Tortora, Nature (London) **425**, 374 (2003).
[9] X. Chen and M. Kamionkowski, Phys. Rev. D **60**, 104036 (1999).
[10] F.-Q. Wu, L.-E. Qiang, X. Wang, and X. Chen, Phys. Rev. D **82**, 083002 (2010).
[11] X. Wang, X. Chen, and C. Park, Astrophys. J. **747**, 48 (2012).
[12] J.-X. Li, F.-Q. Wu, Y.-C. Li, Y. Gong, and X.-L. Chen, Res. Astron. Astrophys. **15**, 2151 (2015).
[13] D. Huterer, D. Kirkby, R. Bean, A. Connolly, K. Dawson, S. Dodelson, A. Evrard, B. Jain, M. Jarvis, E. Linder *et al.*, Astropart. Phys. **63**, 23 (2015).
[14] F.-Q. Wu and X. Chen, Phys. Rev. D **82**, 083003 (2010).
[15] Y.-C. Li, F.-Q. Wu, and X. Chen, Phys. Rev. D **88**, 084053 (2013).
[16] A. Avilez and C. Skordis, Phys. Rev. Lett. **113**, 011101 (2014).
[17] C. Umilt, M. Ballardini, F. Finelli, and D. Paoletti, J. Cosmol. Astropart. Phys. 08 (**2015**) 017.

[18] M. Ballardini, F. Finelli, C. Umilt, and D. Paoletti, J. Cosmol. Astropart. Phys. 05 (**2016**) 067.
[19] M. Ballardini, M. Braglia, F. Finelli, D. Paoletti, A. A. Starobinsky, and C. Umilt, J. Cosmol. Astropart. Phys. 10 (2020) 044.
[20] M. Rossi, M. Ballardini, M. Braglia, F. Finelli, D. Paoletti, A. A. Starobinsky, and C. Umilt, Phys. Rev. D **100**, 103524 (2019).
[21] M. Braglia, M. Ballardini, W. T. Emond, F. Finelli, A. E. Gümrükçüoğlu, K. Koyama, and D. Paoletti, Phys. Rev. D **102**, 023529 (2020).
[22] M. Braglia, M. Ballardini, F. Finelli, and K. Koyama, Phys. Rev. D **103**, 043528 (2021).
[23] I. de Martino, M. De Laurentis, and S. Capozziello, Universe **1**, 123 (2015).
[24] M. Ishak, Living Rev. Relativity **22**, 1 (2019).
[25] B. P. Abbott, R. Abbott, T. D. Abbott, F. Acernese, K. Ackley, C. Adams, T. Adams, P. Addesso, R. X. Adhikari, V. B. Adya *et al.*, Phys. Rev. Lett. **119**, 161101 (2017).
[26] B. P. Abbott, R. Abbott, T. D. Abbott, F. Acernese, K. Ackley, C. Adams, T. Adams, P. Addesso, R. X. Adhikari, V. B. Adya *et al.*, Astrophys. J. **848**, L13 (2017).
[27] B. P. Abbott, R. Abbott, T. D. Abbott, F. Acernese, K. Ackley, C. Adams, T. Adams, P. Addesso, R. X. Adhikari, V. B. Adya *et al.*, Astrophys. J. **848**, L12 (2017).
[28] J. M. Ezquiaga and M. Zumalacárregui, Phys. Rev. Lett. **119**, 251304 (2017).
[29] J. Sakstein and B. Jain, Phys. Rev. Lett. **119**, 251303 (2017).
[30] P. Creminelli and F. Vernizzi, Phys. Rev. Lett. **119**, 251302 (2017).
[31] T. Baker, E. Bellini, P. G. Ferreira, M. Lagos, J. Noller, and I. Sawicki, Phys. Rev. Lett. **119**, 251301 (2017).
[32] A. Casalino, M. Rinaldi, L. Sebastiani, and S. Vagnozzi, Phys. Dark Universe **22**, 108 (2018).
[33] A. Casalino, M. Rinaldi, L. Sebastiani, and S. Vagnozzi, Classical Quantum Gravity **36**, 017001 (2019).
[34] A. Lewis, A. Challinor, and A. Lasenby, Astrophys. J. **538**, 473 (2000).
[35] A. Lewis and S. Bridle, Phys. Rev. D **66**, 103511 (2002).
[36] B. Hu, M. Raveri, N. Frusciante, and A. Silvestri, Phys. Rev. D **89**, 103530 (2014).
[37] A. Hojjati, L. Pogosian, and G.-B. Zhao, J. Cosmology Astropart. Phys. 08 (**2011**) 005.
[38] E. V. Linder, Phys. Rev. D **95**, 023518 (2017).
[39] P. A. R. Ade, N. Aghanim, M. Arnaud, M. Ashdown, J. Aumont, C. Baccigalupi, A. J. Banday, R. B. Barreiro, N. Bartolo *et al.* (Planck Collaboration), Astron. Astrophys. **594**, A14 (2016).
[40] E. Di Valentino, A. Melchiorri, and J. Silk, Nat. Astron. **4**, 196 (2020).
[41] G. Efstathiou and S. Gratton, Mon. Not. R. Astron. Soc. **496**, L91 (2020).
[42] S. Vagnozzi, A. Loeb, and M. Moresco, Astrophys. J. **908**, 84 (2021).
[43] J. Mathews and R. L. Walker, *Mathematical Methods of Physics* (WA Benjamin, New York, 1970).
[44] H. Kodama and M. Sasaki, Prog. Theor. Phys. Suppl. **78**, 1 (1984).
[45] C.-P. Ma and E. Bertschinger, Astrophys. J. **455**, 7 (1995).
[46] W. Hu, U. Seljak, M. White, and M. Zaldarriaga, Phys. Rev. D **57**, 3290 (1998).
[47] T. Tram and J. Lesgourgues, J. Cosmology Astropart. Phys. 10 (**2013**) 002.
[48] B. Audren, J. Lesgourgues, K. Benabed, and S. Prunet, J. Cosmology Astropart. Phys. 02 (**2013**) 001.
[49] T. Brinckmann and J. Lesgourgues, Phys. Dark Universe **24**, 100260 (2019).
[50] N. Aghanim, Y. Akrami, M. Ashdown, J. Aumont, C. Baccigalupi, M. Ballardini, A. J. Banday, R. B. Barreiro, N. Bartolo *et al.* (Planck Collaboration), Astron. Astrophys. **641**, A6 (2020).
[51] N. Aghanim, Y. Akrami, F. Arroja, M. Ashdown, J. Aumont, C. Baccigalupi, M. Ballardini, A. J. Banday, R. B. Barreiro *et al.* (Planck Collaboration), Astron. Astrophys. **641**, A1 (2020).
[52] G. Cheng, Y.-Z. Ma, F. Wu, J. Zhang, and X. Chen, Phys. Rev. D **102**, 043517 (2020).
[53] F. Beutler, C. Blake, M. Colless, D. H. Jones, L. Staveley-Smith, L. Campbell, Q. Parker, W. Saunders, and F. Watson, Mon. Not. R. Astron. Soc. **416**, 3017 (2011).
[54] F. Beutler, C. Blake, M. Colless, D. H. Jones, L. Staveley-Smith, G. B. Poole, L. Campbell, Q. Parker, W. Saunders, and F. Watson, Mon. Not. R. Astron. Soc. **423**, 3430 (2012).
[55] A. J. Ross, L. Samushia, C. Howlett, W. J. Percival, A. Burden, and M. Manera, Mon. Not. R. Astron. Soc. **449**, 835 (2015).
[56] C. Howlett, A. J. Ross, L. Samushia, W. J. Percival, and M. Manera, Mon. Not. R. Astron. Soc. **449**, 848 (2015).
[57] X. Xu, A. J. Cuesta, N. Padmanabhan, D. J. Eisenstein, and C. K. McBride, Mon. Not. R. Astron. Soc. **431**, 2834 (2013).
[58] A. Oka, S. Saito, T. Nishimichi, A. Taruya, and K. Yamamoto, Mon. Not. R. Astron. Soc. **439**, 2515 (2014).
[59] S. Alam, M. Ata, S. Bailey, F. Beutler, D. Bizyaev, J. A. Blazek, A. S. Bolton, J. R. Brownstein, A. Burden, C.-H. Chuang *et al.*, Mon. Not. R. Astron. Soc. **470**, 2617 (2017).
[60] M. Ata, F. Baumgarten, J. Bautista, F. Beutler, D. Bizyaev, M. R. Blanton, J. A. Blazek, A. S. Bolton, J. Brinkmann, J. R. Brownstein *et al.*, Mon. Not. R. Astron. Soc. **473**, 4773 (2018).
[61] P. Zarrouk, E. Burtin, H. Gil-Marín, A. J. Ross, R. Tojeiro, I. Pâris, K. S. Dawson, A. D. Myers, W. J. Percival, C.-H. Chuang *et al.*, Mon. Not. R. Astron. Soc. **477**, 1639 (2018).
[62] D. Huterer, D. L. Shafer, D. M. Scolnic, and F. Schmidt, J. Cosmology Astropart. Phys. 2017 (**2017**) 015.
[63] C. Blake, I. K. Baldry, J. Bland-Hawthorn, L. Christodoulou, M. Colless, C. Conselice, S. P. Driver, A. M. Hopkins, J. Liske, J. Loveday *et al.*, Mon. Not. R. Astron. Soc. **436**, 3089 (2013).
[64] C. Blake, S. Brough, M. Colless, C. Contreras, W. Couch, S. Croom, D. Croton, T. M. Davis, M. J. Drinkwater, K. Forster *et al.*, Mon. Not. R. Astron. Soc. **425**, 405 (2012).
[65] A. Pezzotta, S. de la Torre, J. Bel, B. R. Granett, L. Guzzo, J. A. Peacock, B. Garilli, M. Scodeggio, M. Bolzonella, U. Abbas *et al.*, Astron. Astrophys. **604**, A33 (2017).
[66] T. Okumura, C. Hikage, T. Totani, M. Tonegawa, H. Okada, K. Glazebrook, C. Blake, P. G. Ferreira, S. More, A. Taruya *et al.*, Publ. Astron. Soc. Jpn. **68**, 38 (2016).
[67] D. J. Eisenstein and W. Hu, Astrophys. J. **496**, 605 (1998).

[68] S. Nesseris, G. Pantazis, and L. Perivolaropoulos, Phys. Rev. D **96**, 023542 (2017).
[69] http://pla.esac.esa.int/pla/#home.
[70] M. J. Reid, D. W. Pesce, and A. G. Riess, Astrophys. J. **886**, L27 (2019).
[71] T. M. C. Abbott, F. B. Abdalla, A. Alarcon, J. Aleksić, S. Allam, S. Allen, A. Amara, J. Annis, J. Asorey, S. Avila *et al.*, Phys. Rev. D **98**, 043526 (2018).
[72] H. Akaike, IEEE Trans. Autom. Control **19**, 716 (1974).
[73] Y. Gong and X. Chen, Phys. Rev. D **76**, 123007 (2007).